

February 25, 2003

Optical Seeing at Sierra Negra

Esperanza Carrasco, Alberto Carramiñana,
José Luis Avilés & Omar Yam

*Instituto Nacional de Astrofísica, Óptica y Electrónica,
Luis Enrique Erro 1, Tonantzintla, Puebla 72840, México*

`bec@inaoep.mx`

ABSTRACT

Optical seeing measurements carried out at Sierra Negra, the site of the Large Millimeter Telescope, are reported. The site, one of the highest peaks of Central Mexico, offers good coverage of Northern and Southern hemispheres and we have undertaken several campaigns to investigate the astronomical potential of the site in the optical. Here we report on our campaign aimed at establishing the seeing quality of the site. We present data of the first three campaigns of optical seeing monitoring covering from February 2000 to May 2002, carried out with a Differential Image Motion Monitor. The results clearly indicate a sub-arcsec seeing, better statistics during the dry season and no dependence with the time of night. We find no dependence of our results with the integration time used.

Subject headings: site-testing, atmospheric effects

1. Introduction

Sierra Negra is an extinct volcano in the State of Puebla, Mexico, located at $18^{\circ} 59'06''$ N latitude, $97^{\circ} 18'53''$ W longitude and an altitude of 4580 m above sea level. The mountain is next to Citlaltepetl, the highest peak in Mexico, with just 8 km separating both summits. Sierra Negra is about 100 kms West from the coast of Veracruz in the Gulf of Mexico and 300 kms from the Pacific Coast. The site, administrated by the Instituto Nacional de Astrofísica, Óptica y Electrónica (INAOE), is inside the Pico de Orizaba National Park. Easy access is available via 100 km motorway from the city of Puebla followed by a 20 km access road to the summit. The journey from Puebla city takes about two hours.

In February 1996 Sierra Negra was selected, among more than twenty potential sites, as the site of the Large Millimeter Telescope (LMT/GTM), now under construction. The decision was based on its low atmospheric water vapour content, with registered opacities at 240 GHz down to $\lesssim 0.02$. The LMT/GTM is a 50 m antenna optimised for 1-3 mm observations. First light and science operations are planned for 2005. The LMT/GTM is a bi-national project between Mexico and the United States, leaded by INAOE in Mexico and the University of Massachusetts, at Amherst, in the USA.

With the development of the Sierra Negra site, INAOE planned to measure its quality for optical observations. Because of its altitude and location the site is intrinsically very dry, therefore the conditions are likely to be favorable for near infrared and optical observations. An unknown property of the site is its optical seeing, a key parameter to determine how good an astronomical site is. In the last few decades great efforts have been dedicated to the development of 8-10 m class diameter telescopes and for instrumentation which requires very precise site characterization. Furthermore, the new generation of Extremely Large Telescopes will require selecting sites with very good seeing conditions.

INAOE decided to undertake a first optical seeing and weather measurements campaign starting in February 2000 without basic facilities available. A temporary set-up was prepared for the February campaign, which was in fact the first astronomical night-time work performed at the site. The second campaign started in October 2000, with better facilities such as 5 m tower, a container, a suitable power supply and a place to rest -at about 3000 m above sea level- after observing. From May 2001 we started a routine measurements regime. Here we present the results obtained from February 2000 to May 2002. Weather data have been taken almost continuously from November 2000 up to date. The weather analysis will be reported elsewhere.

2. The Instrument

The data for this work were taken with a Differential Image Motion Monitor (DA/IAC DIMM) developed by Vernin & Muñoz-Tuñon (1995), based on the same physical principle as the ESO DIMM (Sarazin & Roddier 1990) but commercialized by the French company LHESA. The DIMM principle is to produce twin images of a star with the same telescope via two entrance pupils and a wedge. The instrument consists of a 20 cm Celestron telescope, on a very robust equatorial mount, with an intensified CCD camera coupled via an optical fiber bundle to the CCD, a Matrox frame grabber board and a PC. The two $D = 60\text{mm}$ apertures, separated by a distance $d = 140\text{mm}$, are located on a mask attached to the telescope entrance pupil. A precisely cut wedge placed over one of the pupils deviates the

incoming light separating the two star images by approximately 30 arcsec. The intensified CCD camera and the frame grabber register the relative position of both stellar images after computing the centroid position of each. A statistical seeing value is assessed based on the variance of the differential image motion after 200 images are taken. The measurement corresponds roughly to a wavelength $\lambda = 0.5 \mu\text{m}$, as dictated by the response of the system.

Because it is a differential method the technique is, in principle, insensitive to erratic motions of the telescope introduced by wind or ground vibrations. Sarazin & Roddier (1990) showed that, assuming a Kolmogorov power-law spectrum for the turbulent cells, the longitudinal and transverse variances of the differential motion between the images, σ_l and σ_t , are related to the Fried parameter r_0 as:

$$\sigma_l^2 = 2\lambda^2 r_0^{-5/3} [0.179D^{-1/3} - 0.097d^{-1/3}] \quad (1)$$

$$\sigma_t^2 = 2\lambda^2 r_0^{-5/3} [0.179D^{-1/3} - 0.145d^{-1/3}]. \quad (2)$$

Two independent r_0 values are obtained which, in principle, should have the same value. The parameter r_0 can be imagined as the telescope diameter that would produce a diffraction spot of the same size as that produced by the atmospheric turbulence. The seeing is given by $s_{FWHM} = 0.98 (\lambda/r_0)$. These computations are carried out internally by the instrument, providing measures of $s \equiv s_{FWHM}$ derived from the longitudinal and transverse estimates. The DA/IAC DIMM achieves an accuracy better than 0.1" for stars brighter than fourth magnitude with a 10 ms time exposure. A reliable seeing measurement is attained within twenty seconds.

3. Observations and Data

The seeing monitor location at the summit is shown in figure 1. The LMT is located to the left. The circle corresponding to the LMT track is marked and it has 40 meters of diameter. The approximate location of the seeing monitor and weather station is marked by the black square, to the North-East of the LMT. The DIMM and the weather station are on a five meter height tower to avoid the surface layer (Vernin & Muñoz-Tuñon 1994). The DIMM is on a tower independent of the platform where the observers move freely without affecting the seeing measurement. The tower is near a sharp edge to face directly the incoming winds. Thermal equilibrium is ensured by the absence of an enclosure.

The data available cover 85 nights, grouped in three sets: 4 nights between February 22nd and April 7th, 2000, corresponding to the first campaign; a second one with 10 observing nights between October 23rd and December 13th 2001; and the third campaign which

consisted of 71 nights from May 24th, 2001 to May 3rd, 2002. We observed bright stars, almost always $m_V \lesssim 2.5$.

The high-altitude and precarious initial development of the site made the initial runs a real challenge. Nevertheless we successfully carried out measurements, for the first time, during the night at the summit. To compare all measurements, we present statistics giving equal weight to every data point. For the analysis we only consider data files with at least 20 points acquired close to the zenith (airmass ≤ 1.15) with non-saturated images (DIMM parameter $\text{pixmax} \leq 255$) to ensure a reliable stellar centroid determination.

3.1. Results on seeing statistics

Figure 2 is the daily plot of all the measurements. The dots are the median and the error bars go from the first to the third quartile. The central dotted line denotes the seeing median for the all data set, corresponding to 0.78". The top dotted line is the distribution third quartile, 1.05" and the bottom dotted line is the first quartile, corresponding to 0.62". The histogram and the cumulative distribution of the same data are shown in figure 3. It can be appreciated a sub-arcsec seeing 75% of the time.

To investigate the seeing seasonal behaviour we define the dry season from November to April and the wet season from May to October. The histogram and cumulative distribution for the dry and the wet seasons are shown in figures 4 and 5 respectively. While the seeing median during the dry season is 0.75", for the wet season it raises 0.92". However it should be noticed that during August 2001 the seeing was specially bad (with a median of 1.49"; see table 1). To study the August contribution to the seeing we made the exercise of calculating statistics for the wet season without August 2001, the seeing median becoming 0.78", significantly closer to the dry season seeing median.

To compare the monthly seeing behaviour we present, in table 1, statistics giving equal weight to each individual seeing measurement for the complete data set: the first column is the month, the next three columns give the details of the data acquired *i.e.* number of nights, number of observing hours during those nights and number of points. The next columns give the data statistics: mean, standard deviation, minumuum value, first quartile, median and third quartile. The global statistics shows that for 85 observing nights spanning from February 2000 to May 2002, the seeing median is 0.78" with a standard deviation of 0.44".

In figure 6 the distribution of seeing values as a function of UT is shown for the 85 observing nights. The dots represents the median for each hour and the error bars go from the first to the third quartile. The histogram is shown in the upper panel. It must be noted

that the first bin, corresponding to 7-8 PM local time, has only a few points so the high seeing value might be due to low number statistics rather than a intrinsically higher seeing at the beginning of the night. We conclude that our data do not show any systematic trend along the night. Muñoz-Tuñon, Vernin, & Varela (1997) observed that there is no general trend in the seeing evolution for the Roque de los Muchachos Observatory. In contrast Giovanelli et al. (2001), point out that for high altitude cordillera sites, in northern Chile, the seeing tends to be of lower quality at the beginning of the evening.

3.2. The seeing integration time

It has been discussed by several authors that the temporal averaging of the variance of the differential motion with a finite exposure time depends on the average velocity and the direction of displacement of the wavefront corrugation with respect to the DIMM aperture (Martin 1987; Sarazin & Tokovinin 2001). Giovanelli et al. (2001), on high altitude cordillera sites in Chile, measure the seeing alternating 10 msec and 20 msec exposures. They obtain seeing estimates derived from 10 msec exposures, from 20 msec exposures and extrapolations to “zero exposure”, obtained by multiplying the 10 msec seeing by the ratio of the 10 and 20 msec measurements. They find that the median values of the 0 ms seeing vary between 0.66” and 0.76”, those of the 10 msec seeing between 0.56” and 0.65” while those of the 20 msec between 0.48” and 0.56”. According to these authors, the seeing for the 10 msec series is statistically worse than that for the 20 msec series, as the latter smears the image motion somewhat.

Our DIMM has a default integration time of 20 msec. The first data set that spans from February 2000 to August 2001 were taken using that integration time. During the next 12 observing nights we alternated measurements with 10 and 20 msec integration times. The camera control allows the user to alternate between the default time and a mechanically selected integration time. As the selection is manual we decided to take 15 integrations at each integration time. The results are shown in Figure 7 where the seeing as a function of time is shown for each night. The filled circles corresponds to the medians of the 10 msec integration samples while the open circles to the medians of the 20 msec samples. Qualitatively, there is no significant difference between the trends of both data sets. We compare quantitatively the samples by plotting the 10 msec seeing medians *vs.* 20 msec seeing medians where each data set has been interpolated through a spline fit to overlap in time the other data set, such that at each time we have one data point (either from the 10 msec or 20 msec sample) and one spline interpolation (from the 20 msec or 10 msec sample) which can be compared. The comparison is shown in figure 8, where the best fit to the data is the dotted line and the

full line represents $s_{10} = s_{20}$. The best fit slope (0.89 ± 0.20) and intercept (0.10 ± 0.15) are compatible with $s_{10} = s_{20}$.

We also compared the complete distributions of 10 ms and 20 ms integration times seeing values, shown in figure 9. A χ^2 comparison test between both distribution gives $\chi^2 = 64.8$ for 46 degrees of freedom, that is a 3.5% probability that both distributions are the same. However, if we compare both distributions with the common distribution, derived from putting together the samples, then the respective χ^2 values are 10.1 and 12.1 for the same number of degrees of freedom, giving respective probabilities of $1 - (4 \times 10^{-9})$ and $1 - (10^{-7})$ that each distribution can be derived from the same parent distribution. As it can be appreciated in the two lower panels of figure 9, the two distributions of seeing values are compatible with a single parent distribution. The total seeing median including both integration times is $0.77''$.

Following a suggestion by Marc Sarazin (private communication), we studied the presence of temporal averaging effects on our seeing measurements by comparing the seeing median *vs.* the wind velocity at 200 mb using the NOAA Global Gridded Upper Air data base, for each night of our 20 msec sample. The results are shown in the upper panel of Figure 10. The seeing error bars go from the first to the third quartile. The wind data are daily average of four measurements available on the NOAA database. The dotted line represents the best least square linear fit, consistent with slope equal to zero within 1.1σ . The correlation coefficient is equal to -0.227 and the rms dispersion is $0.359''$. The errors were obtained using a bootstrap technique. The data show that the seeing does not drop at high speed as it would be expected in the presence of temporal averaging effects. In the lower panel of the same figure, the 10 ms seeing data are shown. In this case the best fit is also consistent with zero slope, within 1.5σ , and the correlation coefficient is -0.274 .

To study the presence of any correlation between seeing and wind velocity at ground level, we compare the seeing and wind velocity daily medians at the site. The wind velocity was measured with a meteorological station located on the seeing monitor tower. Figure 11 shows the seeing median as a function of the wind velocity median for those nights that have simultaneous seeing and wind velocity data. The seeing error bars go from the first to the third quartile. The wind velocity distribution median was calculated from the data obtained between 8:pm and 6:am local time, the error bars corresponding to the first and third quartile are not included in the plot for clarity. In the upper panel the results for 17 nights of the 20 msec sample are shown. The dotted line represents the best fit that is consistent with zero slope within 1.4σ , a correlation factor equal to -0.435 and a rms dispersion of $0.384''$. In the lower panel the data obtained for 50 nights of the 10 ms sample are shown. The best fit is consistent with slope equal to zero within 1.1σ , a correlation factor of 0.281 and a rms

dispersion equal to $0.256''$.

In contrast with Giovanelli et al. (2001) results on high altitude cordillera sites in Chile, the data for Sierra Negra suggest that, within our statistics, there is no difference between the 10 msec and the 20 msec series. It must be noted that Vernin & Muñoz-Tuñon (1995) find the seeing bias produced by the difference in exposure time to be highly dependent on the magnitude of the star. As we generally use stars brighter than $m_V = 2$, it is possible that this bias is in our data but below measurable error, therefore not influencing our results. Nevertheless from December 2001 onwards all our measurements are made using 10 msec exposures.

4. Conclusions

We present the first seeing measurements carried out at Sierra Negra. For 85 observing nights, seeing values of $0.62''$ were achieved 25% of the time, below $0.78''$ during 50% of the time, and sub-arcsec seeing for 70% of the time. The comparison between the dry and the wet season shows that the seeing median is better during the dry season with a value of $0.73''$ and sub-arcsec seeing 77% of the time. In contrast for the wet season the seeing median is $0.92''$ value is strongly affected by August 2001 contribution. We analysed the dependence of the seeing statistics with time of night without finding any systematic trend of seeing as a function of time. We did not find any correlation between the seeing values and the 200 mb wind velocity. A preliminary analysis of the correlation between the seeing and the wind velocity at ground level was carried out. The results show that there is not an obvious correlation between them. Nevertheless we will continue analysing the seeing as a function of other meteorological parameters in more detail to try to find out where most of the turbulence is concentrated.

The results obtained so far show that Sierra Negra is a competitive site for optical astronomy. We will continue with our seeing and meteorological measurements to characterise the site on a longer time scale basis. We have carried out an independent analysis of the seeing temporal structure and the results will be reported in a separated paper.

We thank R.J. Terlevich his interest and his useful comments and suggestions. This study was possible through funds from the Instituto Nacional de Astrofísica, Óptica y Electrónica. The 20mb wind velocity data was provided by the NOAA-CIRES Climate Diagnostics Center, Boulder, Colorado, USA, from their Web site at <http://www.cdc.noaa.gov/>.

REFERENCES

Giovanelli, R., Darling, J., Sarazin, M., Yu, J., Harvey, P., Henderson, Ch., Hoffman, W., Keller, L., Barry, D., Cordes, J., Eikenberry, S., Gull, G., Harrington, J., Smith, J. D., Stacey, G., & Swain, M. 2001 PASP 113, 789.

Martin, H. M. 1987, PASP 99, 1360.

Muñoz-Tuñon, C., Vernin, J. & Varela, A. M., 1997, A&AS 125, 183.

Sarazin, M. & Roddier, F., 1990, A&A 227, 294.

Sarazin, M. & Tokovinin A., 2001, Proceeding of Beyond Conventional Adaptive Optics, Venice 7-10, 2001, eds. R. Raggazoni, N. Hubin, & S. Esposito.

Vernin, J. & Muñoz-Tuñon, C., 1994, A&A 284, 311.

Vernin, J. & Muñoz-Tuñon, C., 1995, PASP 107, 265.

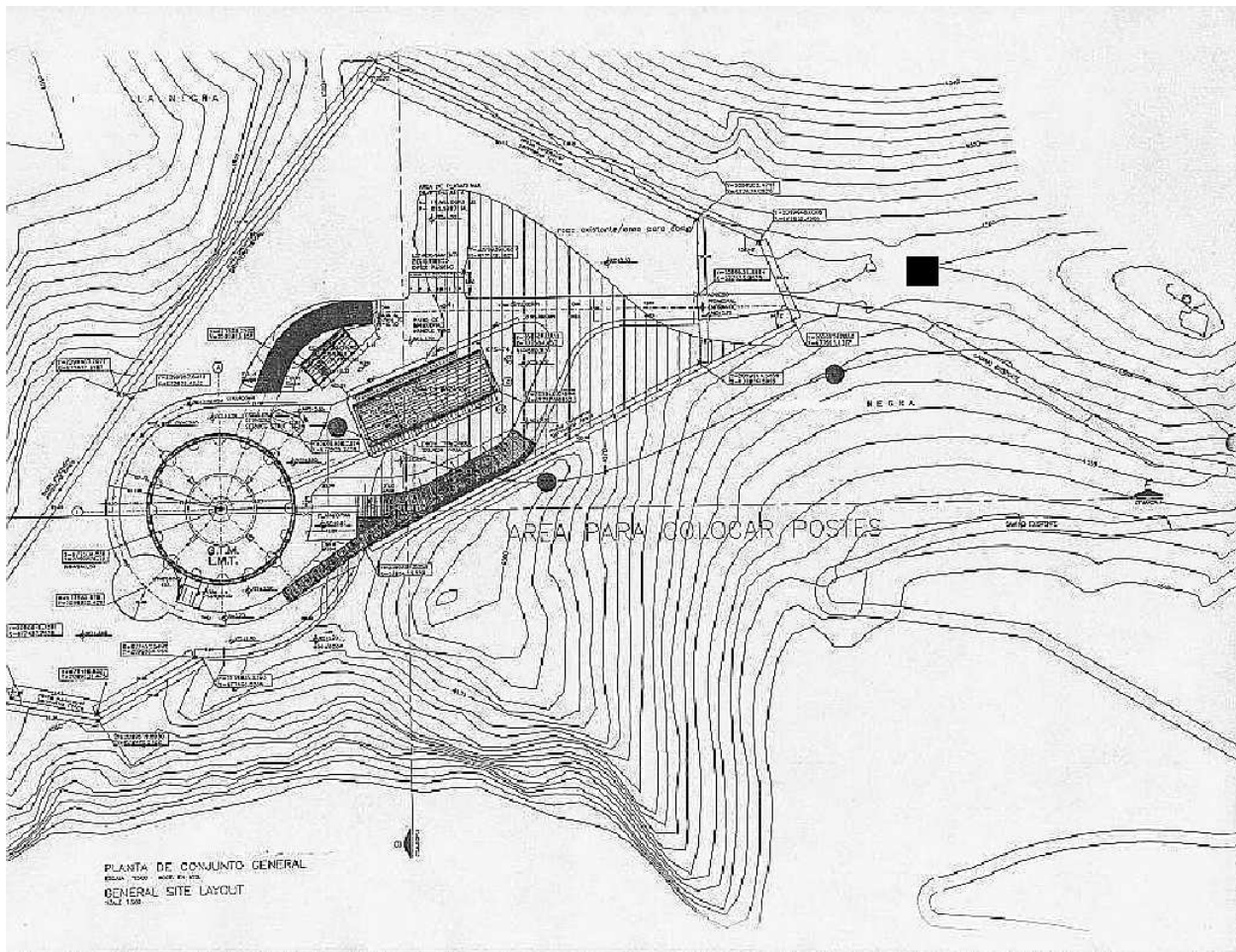


Fig. 1.— Layout of the Large Millimeter Telescope site. North is up and East to the right. The LMT track is marked by the 40 m diameter dark circle located at the middle left. The approximate location of the seeing monitor and weather station is marked by the black square, East-North-East of the LMT construction.

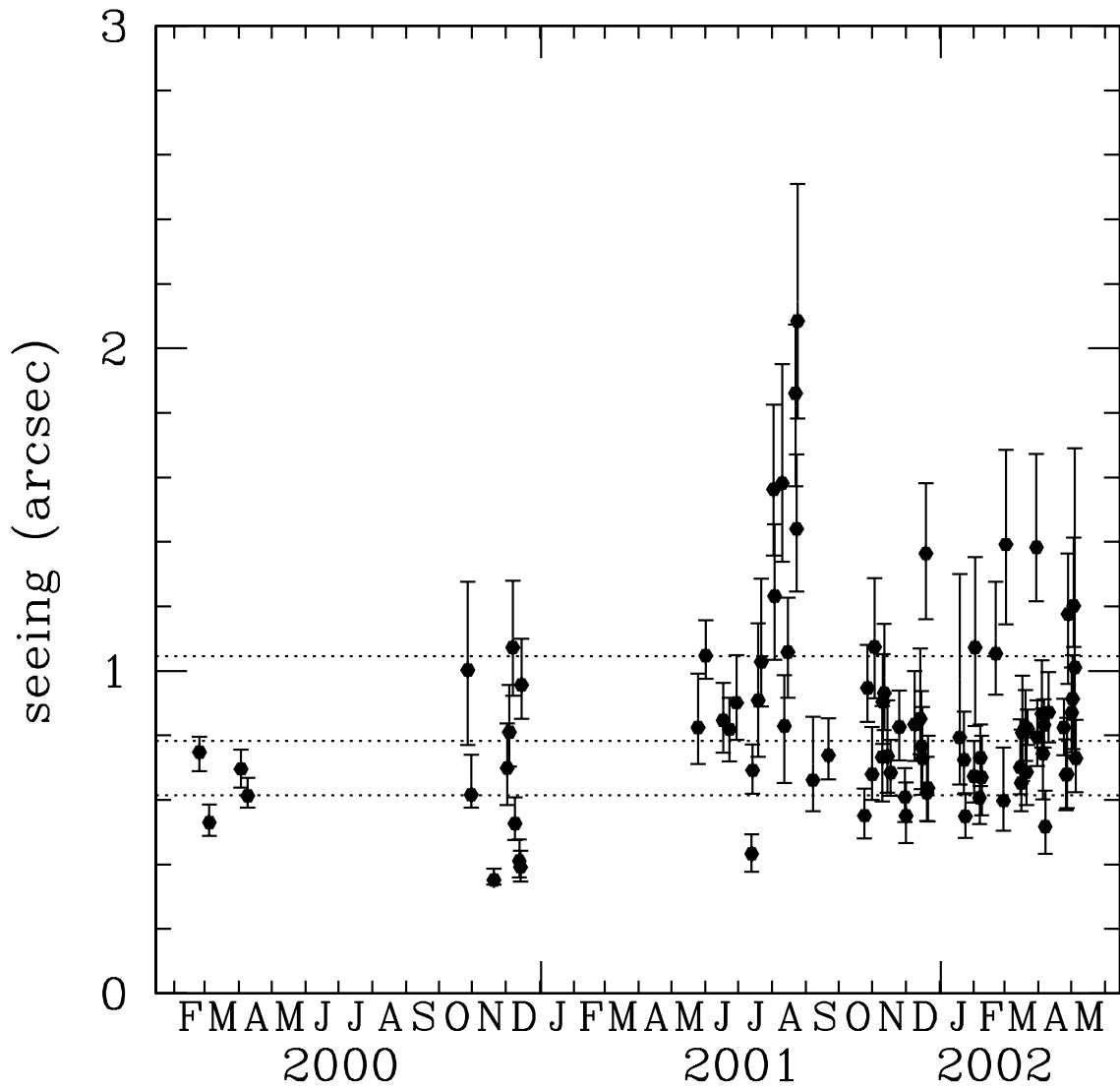


Fig. 2.— Seeing daily statistics for all data points. The dots are the median and the error bars go from the first to the third quartile. The central dotted line denotes the seeing median for the whole data set, corresponding to **0.78"**. The top dotted line is the distribution third quartile, equal to **1.04"**, and the bottom dotted line is the first quartile, corresponding to **0.61"**.

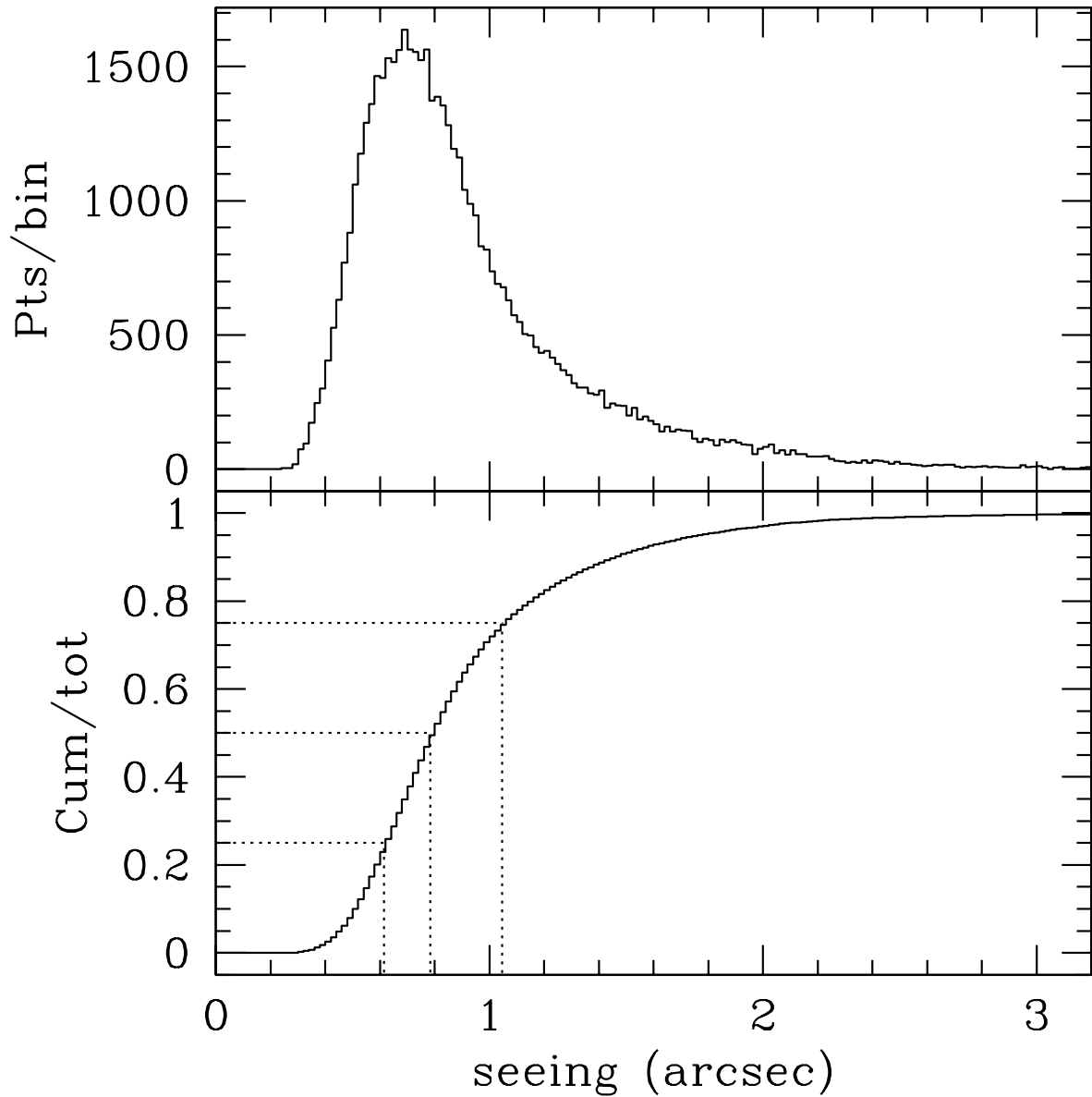


Fig. 3.— Seeing histogram (*top*) and cumulative (*bottom*) distribution of all data points. The global statistics show that for 85 observing nights spanning from February 2000 to May 2002. Seeing values of $0.61''$ were achieved 25% of the time, seeing below $0.78''$ during 50% of the time and sub-arcsec seeing 70% of the time.

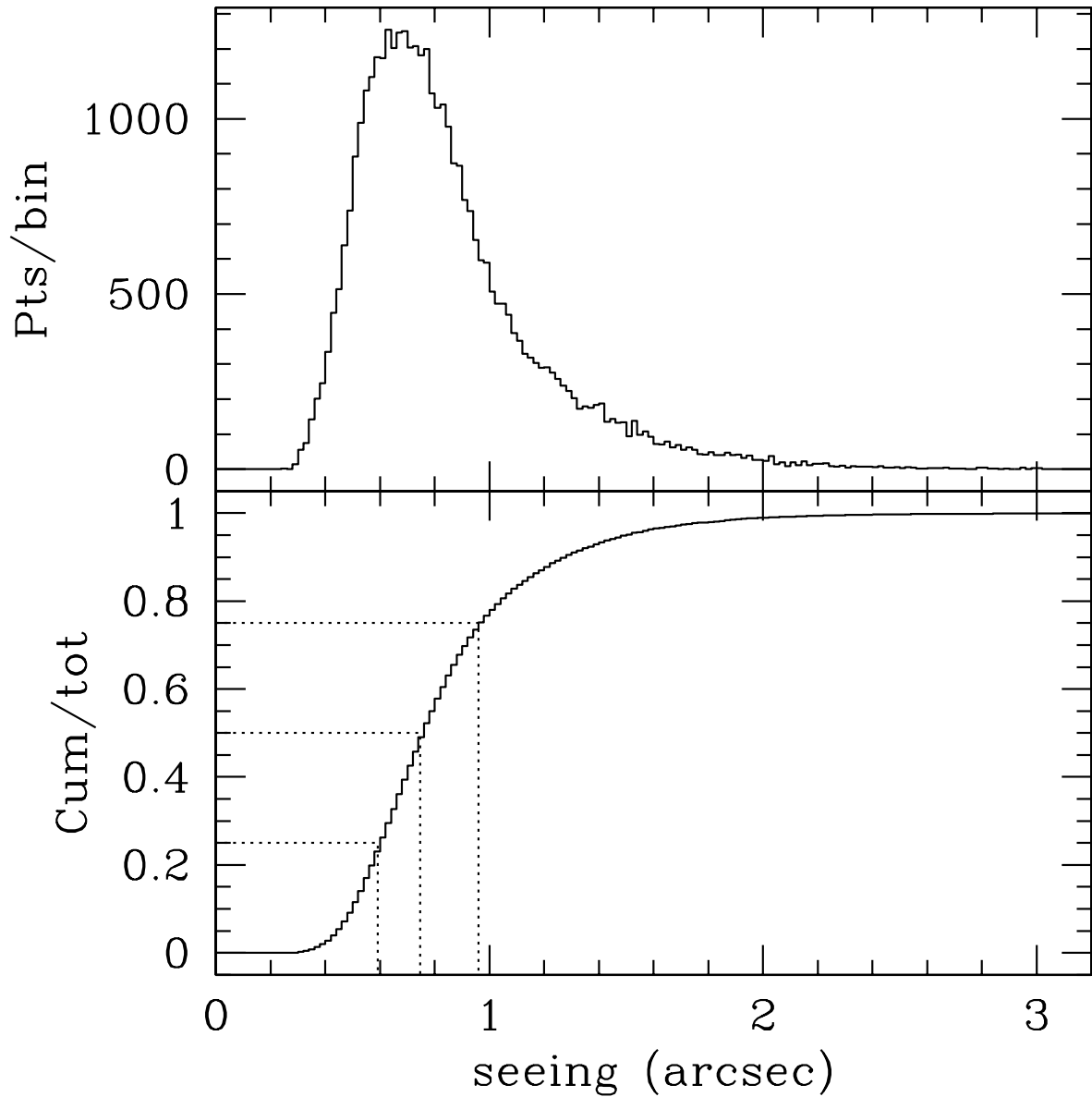


Fig. 4.— Histogram (*top*) and cumulative (*bottom*) seeing distribution for the **dry season** *i.e.* from November to April. The seeing median, indicated by the central dotted line, is **0.75"**. The distribution first quartile, equal to **0.59"**, and the third quartile value, equal to **0.96"**, are indicated by the bottom and top dotted lines respectively.

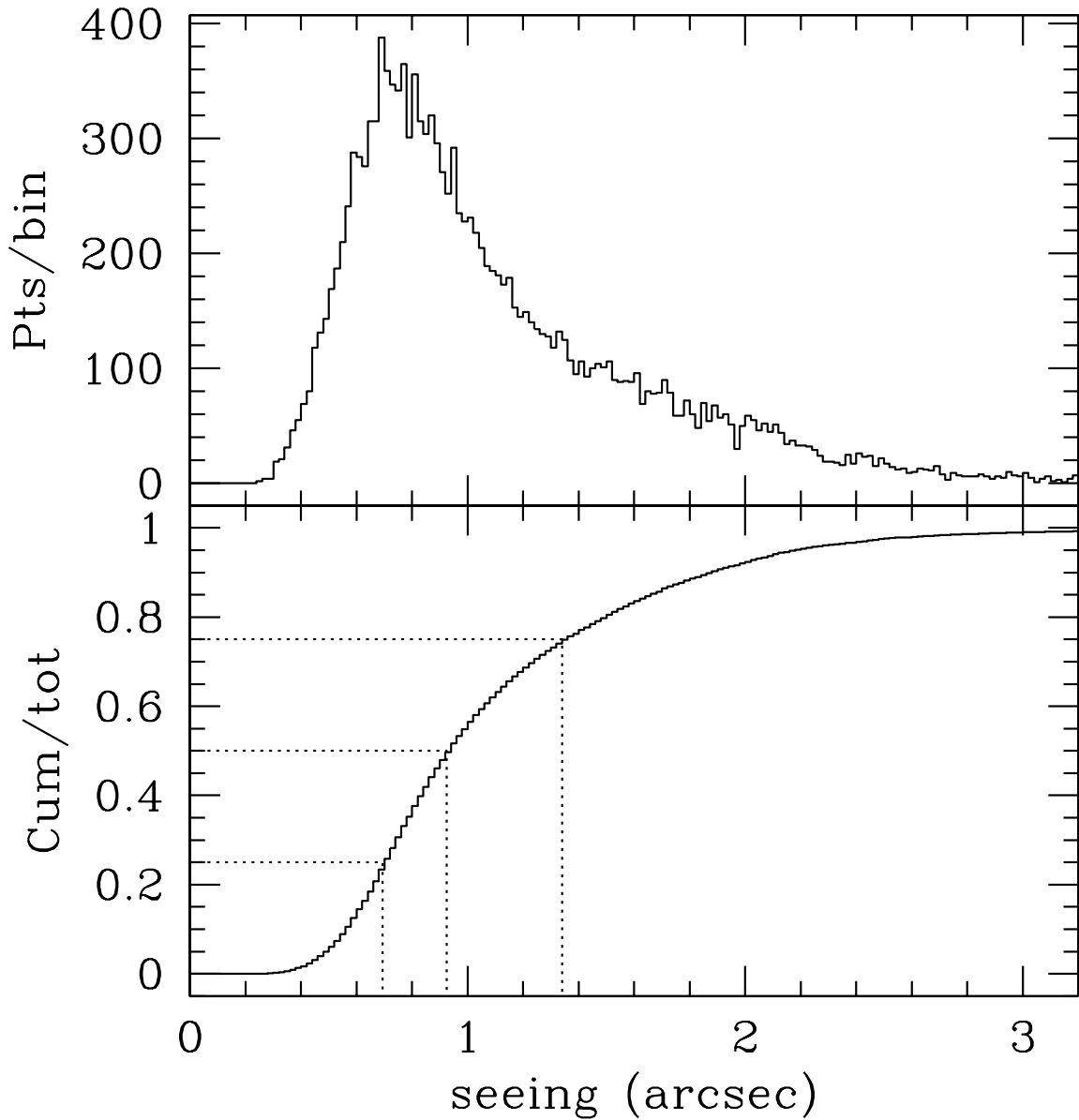


Fig. 5.— Histogram (*top*) and cumulative (*bottom*) seeing distribution for the **wet season**, *i.e.* from May to October. The seeing median, indicated by the central dotted line is **0.92"**. The bottom dotted line corresponds to the first quartile value, equal to **0.69"**, and the third quartile value, equal to **1.34"**, is indicated by the top dotted line.

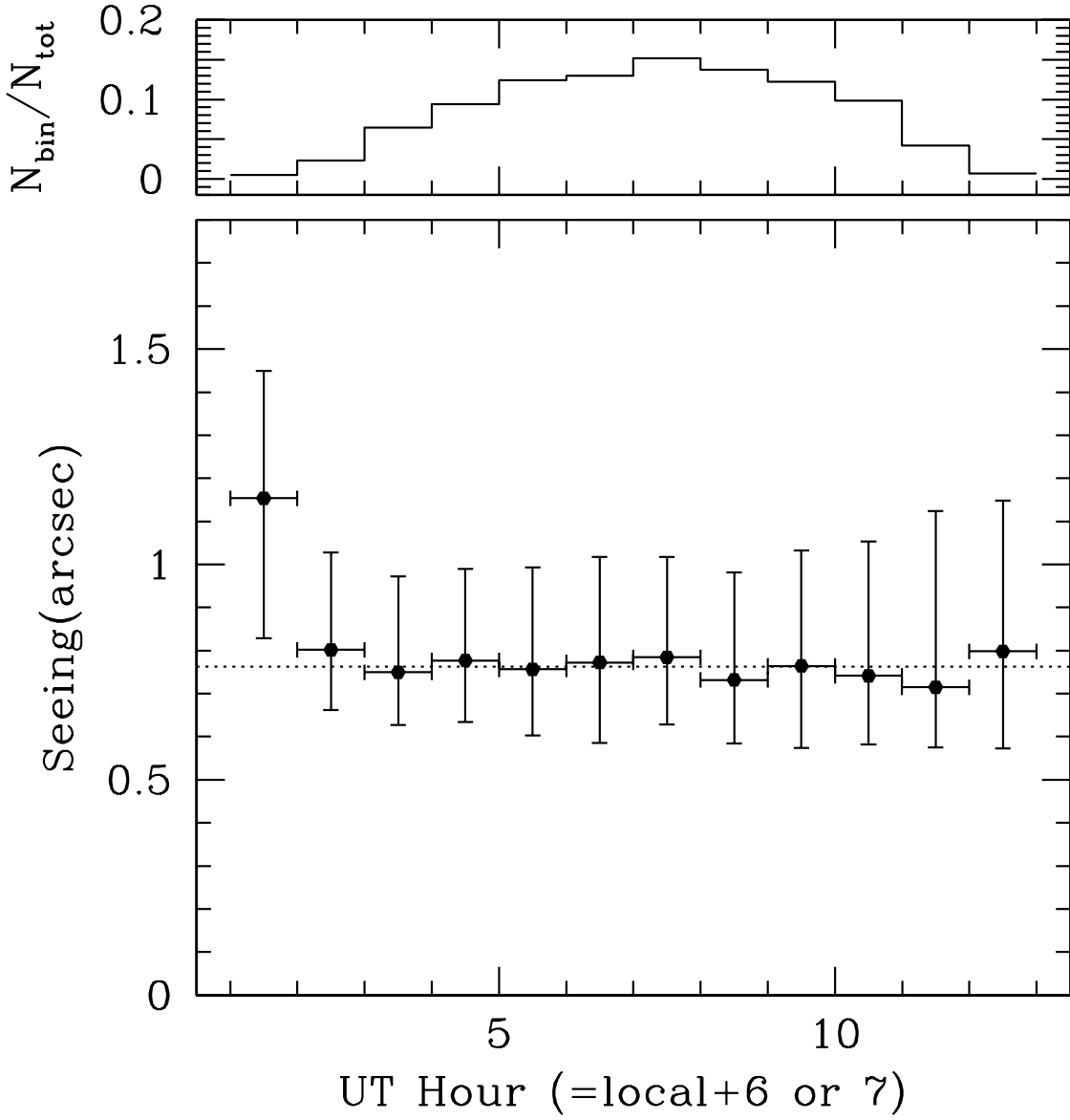


Fig. 6.— Distribution of seeing values for different hours of the night (in UTC). The dots mark the median values while the error bars go from the first to the third quartile. The upper panel shows the number of data points for each hour interval. Note that the 1-2 hrs UTC bin (7-8:pm local) has a much lower coverage than the middle of the night, so the deviation of uniformity for that bin might be apparent and due to low number statistics (*i.e.* dominated by one or two nights with bad seeing). The data are basically consistent with no systematic trend during the night.

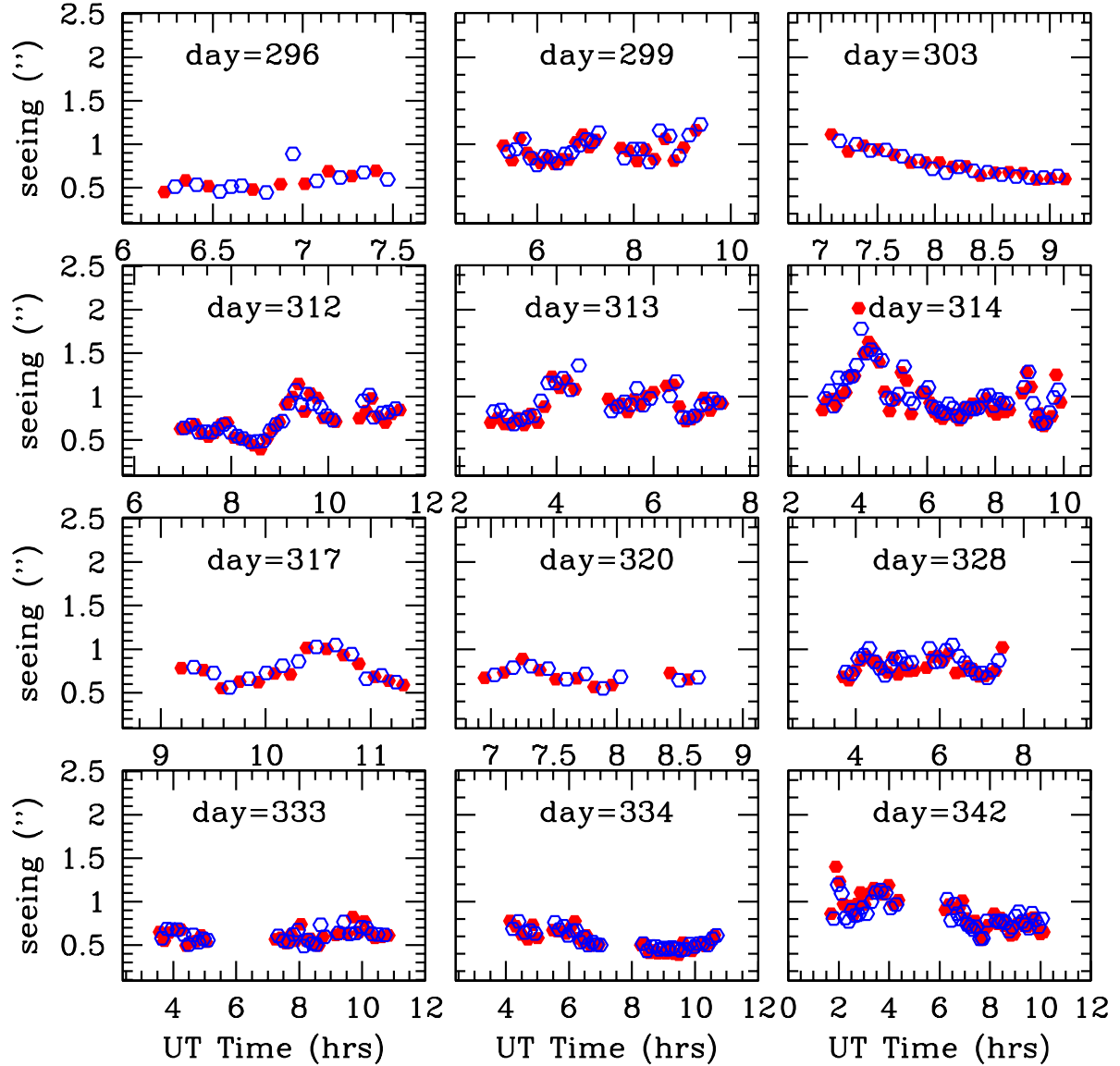


Fig. 7.— Seeing time profiles for 12 nights with samples of 15 seeing measurements taken alternating with 10 msec and 20 msec integration times. Each point in the figure represents the median over each sample, distinguishing between 10 msec samples (filled circles) and 20 msec samples (open circles). There is no clear qualitative systematic difference between both data, all taken in 2001.

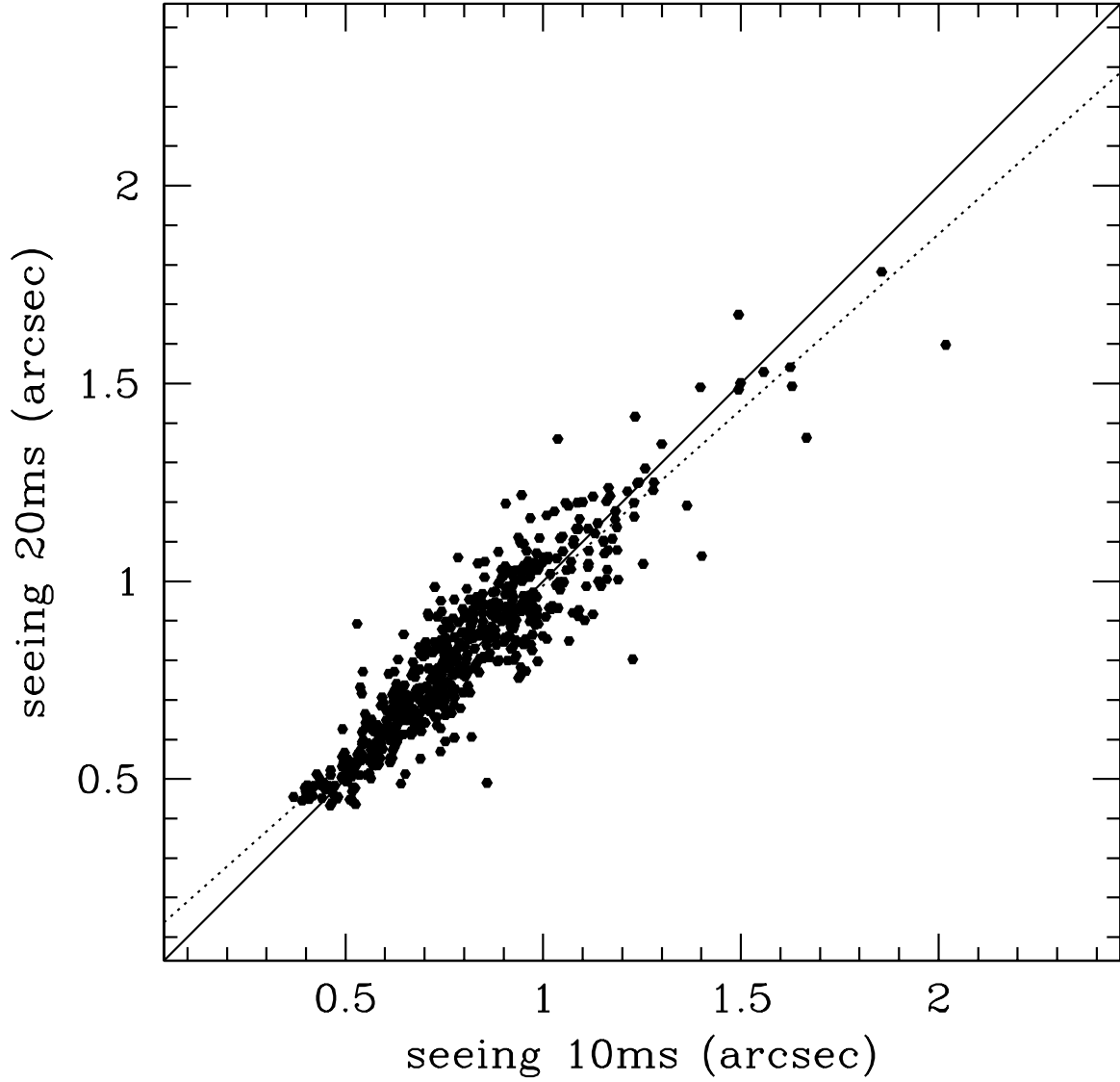


Fig. 8.— Comparison of seeing data taken with integration times of 10 and 20 msec. Each data set has been extended through a spline fit to overlap in time the other data set, so that each point represents one sample (either 10 msec or 20 msec) and the reciprocal spline interpolation (from the 20 msec or 10 msec data). The full line represents $s_{10} = s_{20}$ while the dotted line is the best fit to the data: $s_{20} = (0.888 \pm 0.205)s_{10} + (0.102 \pm 0.152)$, with a correlation of 0.92 and rms=0.08". Errors were determined with the bootstrap method.

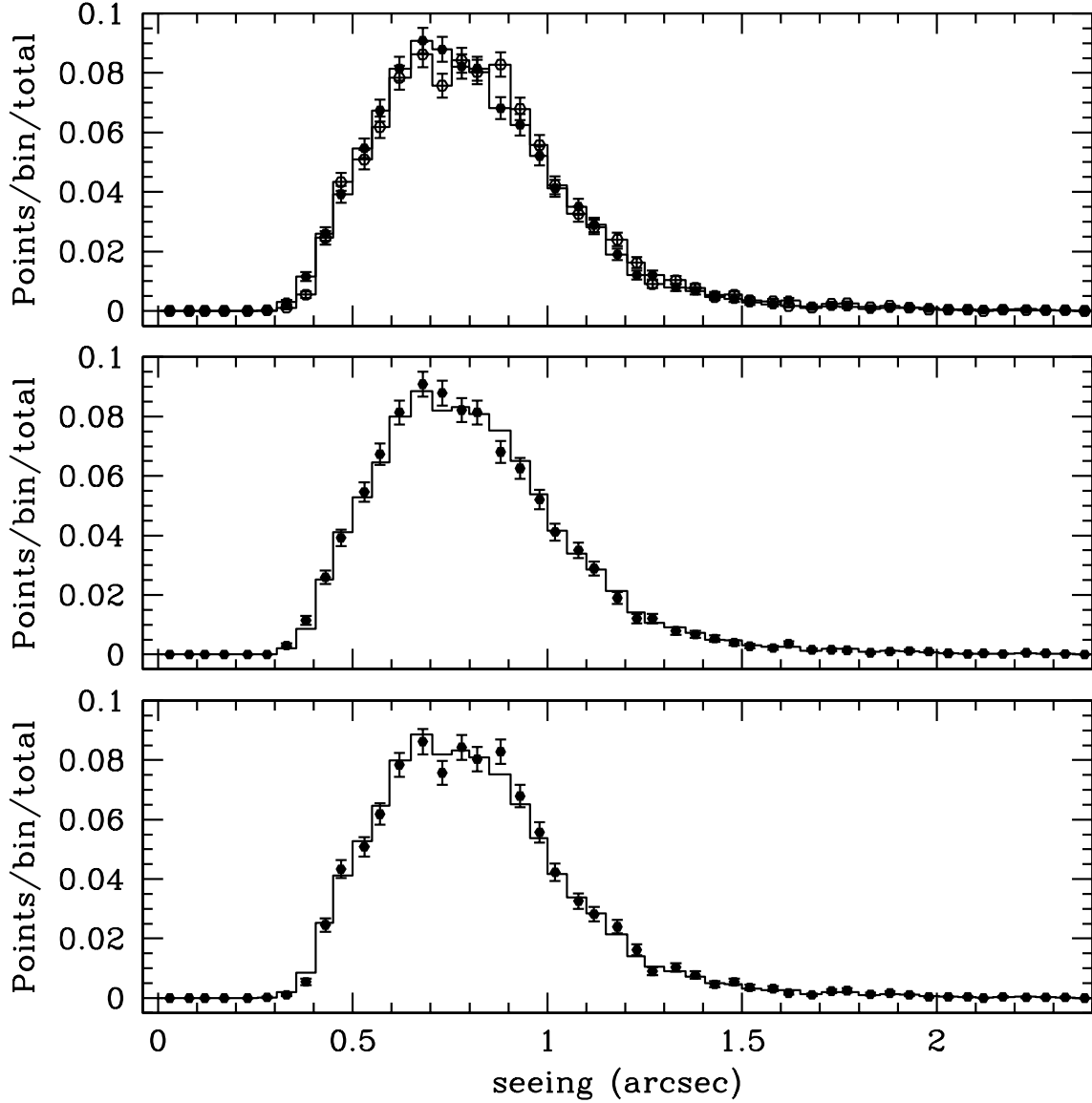


Fig. 9.— Comparison between the distributions of s_{10} and s_{20} values (*top*); between the common distribution and s_{10} values (*middle*); and between the common distribution and s_{20} values (*bottom*). As expected from the figure, the quartile and median values are similar. In particular $q_2(s_{10}) = 0.76''$, $q_2(s_{20}) = 0.78''$ and $q_2(s_{10}\&s_{20}) = 0.77''$. Both s_{10} and s_{20} distributions are compatible with the same single parent distribution.

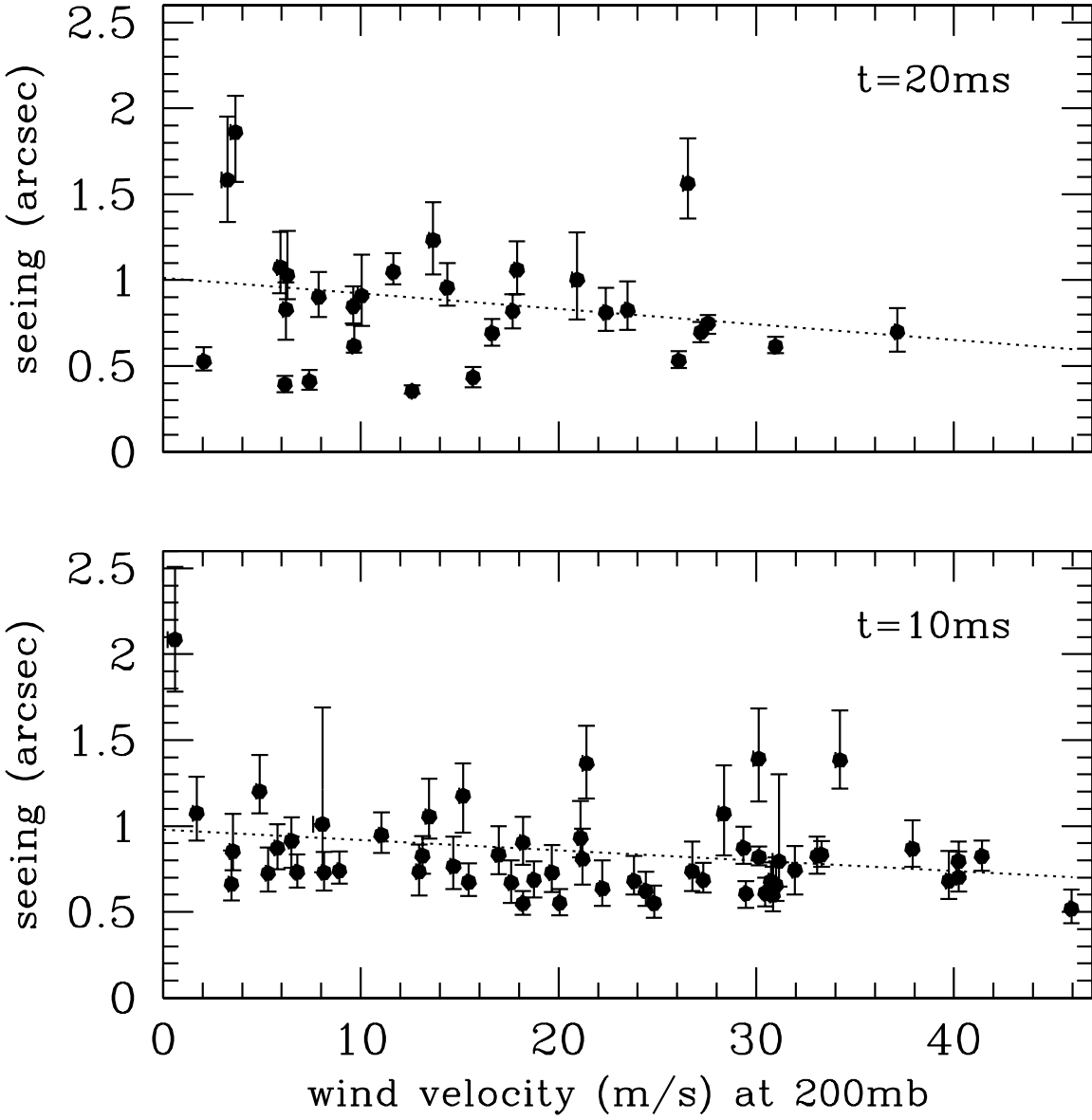


Fig. 10.— Seeing median as a function of the wind velocity at 200 mb. The seeing error bars go from the first to the third quartile. The daily average wind velocities were obtained from the NOAA Global Gridded Upper Air data base. Seeing data for the 20 ms sample (*top*): the dotted line represents the best linear fit, of slope $= -0.009 \pm 0.008$, consistent with a zero slope within 1.1σ . The correlation coefficient is equal to -0.274 and a rms dispersion is $0.260''$. Seeing data for the 10 ms sample (*bottom*): the best linear fit, slope $= -0.006 \pm 0.004$, is consistent with a slope equal to zero within 1.5σ . The correlation coefficient is -0.227 and the rms dispersion $0.359''$.

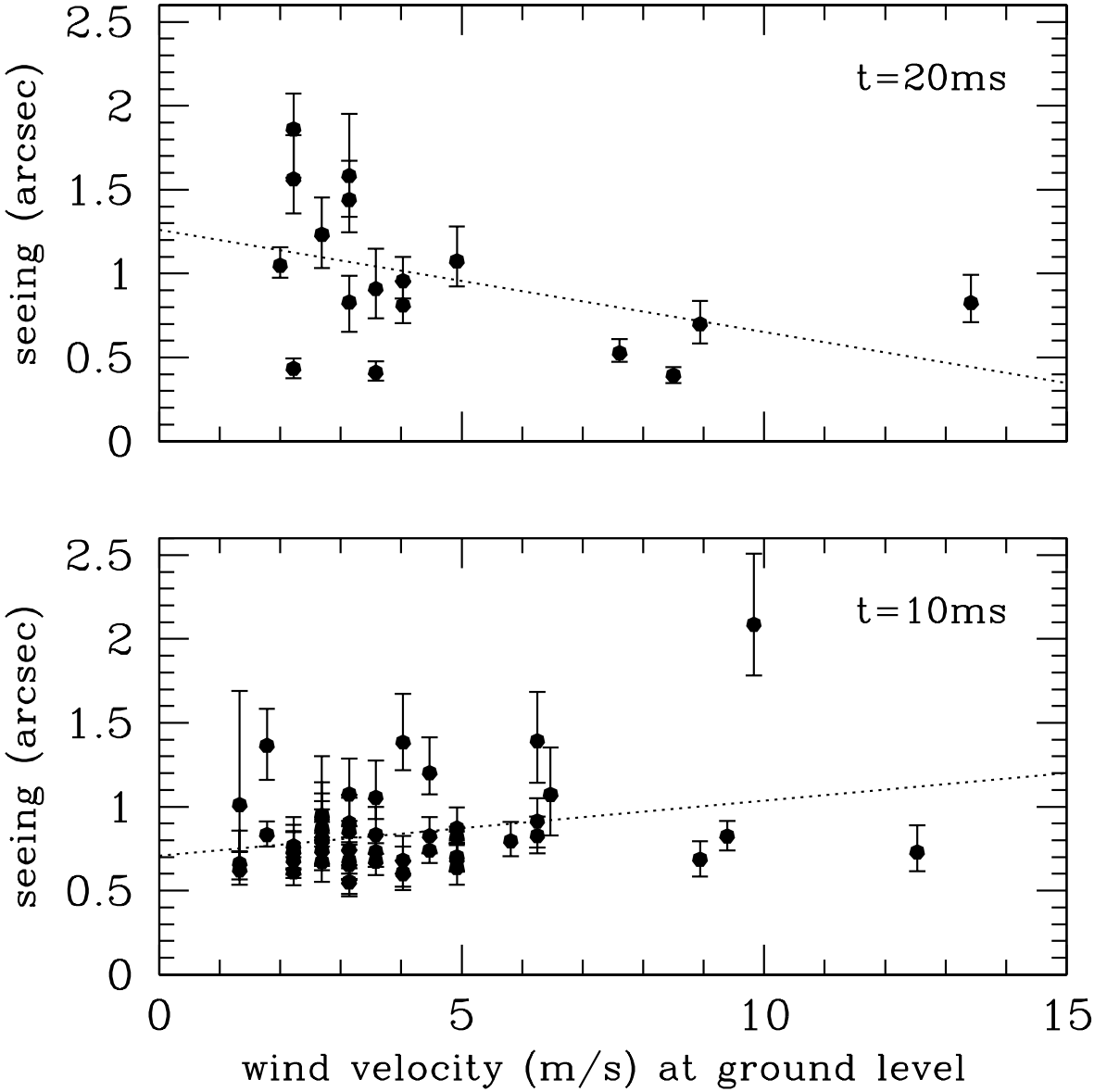


Fig. 11.— Seeing median as a function of the wind velocity median at ground level for those nights that have both seeing and wind velocity data. The seeing error bars go from the first to the third quartile, while the wind velocity error bars are not included for clarity. Seeing data for 17 nights of the 20 ms sample (*top*): the dotted line represents the best linear fit, slope = -0.06 ± 0.04 , which is consistent with a null slope within 1.4σ . The correlation coefficient is -0.435 and a rms dispersion $0.384''$. Seeing data for 50 nights of the 10 ms sample (*bottom*): the best fit, slope = 0.03 ± 0.03 , is also consistent with a slope = 0 within 1.1σ . The correlation coefficient is 0.281 and the rms dispersion $0.256''$.

Table 1. Global statistics per month considering equal weight per each seeing datum.

Date Month Year	Data acquired			Data statistics (")					
	Nights	Hours	Points	Mean	σ	Min	q_1	Median	q_3
Feb 2000	1	0.3	42	0.756	0.087	0.606	0.689	0.748	0.795
Mar 2000	1	1.2	227	0.541	0.077	0.397	0.488	0.531	0.586
Apr 2000	2	1.5	205	0.650	0.132	0.482	0.578	0.631	0.696
Oct 2000	2	2.3	389	1.035	0.344	0.460	0.744	0.958	1.259
Nov 2000	2	3.5	427	0.701	0.204	0.290	0.553	0.678	0.824
Dec 2000	6	25.5	2383	0.661	0.354	0.238	0.401	0.506	0.894
May 2001	2	1.7	302	0.887	0.204	0.552	0.722	0.854	1.021
Jun 2001	3	7.5	1178	0.910	0.468	0.466	0.749	0.848	0.965
Jul 2001	4	12.0	1926	0.736	0.374	0.229	0.488	0.670	0.870
Aug 2001	8	26.7	4467	1.589	0.602	0.476	1.172	1.489	1.894
Sep 2001	2	6.0	1063	0.783	0.307	0.329	0.576	0.677	0.857
Oct 2001	3	15.2	2009	0.811	0.258	0.376	0.616	0.789	0.962
Nov 2001	9	37.6	7352	0.826	0.312	0.290	0.622	0.776	0.959
Dec 2001	7	37.5	6380	0.835	0.326	0.343	0.614	0.755	0.963
Jan 2002	4	29.6	3837	0.782	0.342	0.326	0.574	0.679	0.840
Feb 2002	6	36.0	4207	0.861	0.404	0.272	0.602	0.758	1.002
Mar 2002	9	36.1	4867	0.980	0.431	0.293	0.669	0.846	1.203
Apr 2002	10	44.1	7616	0.788	0.284	0.274	0.588	0.742	0.913
May 2002	4	17.9	3202	0.972	0.447	0.347	0.675	0.834	1.100
All data	85	342.1	52079	0.898	0.441	0.229	0.615	0.784	1.046